Statics and dynamics of an inhomogeneously nonlinear lattice

Debra L. Machacek,[1] Elizabeth A. Foreman,[1] Q. E. Hoq,[2] P. G. Kevrekidis,[1] A. Saxena,[3]
D. J. Frantzeskakis,[4] and A. R. Bishop[3]
[1]*Department of Mathematics, University of Massachusetts, Amherst, Massachusetts, 01003-4515, USA*
[2]*Department of Mathematics, Western New England College, Springfield, Massachusetts 011119, USA*
[3]*Theoretical Division and Center for Nonlinear Studies, Los Alamos National Laboratory, Los Alamos, New Mexico 87545, USA*
[4]*Department of Physics, University of Athens, Panepistimiopolis, Zografos, Athens 15784, Greece*
(Received 17 February 2006; revised manuscript received 29 June 2006; published 5 September 2006)

We introduce an inhomogeneously nonlinear Schrödinger lattice, featuring a defocusing segment, a focusing segment and a transitional interface between the two. We illustrate that such inhomogeneous settings present vastly different dynamical behavior in the vicinity of the interface than the one expected in their homogeneous counterparts. We analyze the relevant stationary states, as well as their stability, by means of perturbation theory and linear stability analysis. We find good agreement with the numerical findings in the vicinity of the anticontinuum limit. For larger values of the coupling, we follow the relevant branches numerically and show that they terminate at values of the coupling strength which are larger for more extended solutions. The dynamical development of relevant instabilities is also monitored in the case of unstable solutions.

DOI: 10.1103/PhysRevE.74.036602 PACS number(s): 05.45.Yv, 03.75.Lm, 63.20.Pw

I. INTRODUCTION

In the past two decades, the number of applications of discrete, nonlinear dynamical models has increased dramatically. A diverse set of applications has emerged, ranging from the nonlinear optics of guided waves in inhomogeneous optical structures [1,2] and photonic crystal lattices [3,4] to atomic physics and the dynamics of Bose-Einstein condensate (BEC) droplets in periodic (optical lattice) potentials [5–8] and from condensed matter, in Josephson-junction ladders [9,10], to biophysics, in various models of double-stranded DNA [11,12]. This broad span of research areas and corresponding applications has now been summarized in a variety of reviews [13–17].

A model that has drawn a particular focus among these areas of applications is the so-called discrete nonlinear Schrödinger equation (DNLS) [16]. This model was first proposed in the context of nonlinear optics, where it describes beam dynamics in coupled waveguide arrays [18,19], but is equally applicable in other settings, such as the dynamics of BEC's confined in deep optical lattices [8,20]. The relevant model involves the nearest-neighbor coupling between adjacent waveguides (wells of the optical lattice in BEC's) and the local nonlinear self-action induced by the Kerr effect in each waveguide (or the mean-field interatomic interaction in the condensate setting).

Typically, the above setup is homogeneous in that all waveguides or wells are identical. However, recently there has been a surge of activity motivated by the experimental tunability of the properties of individual waveguides and wells. In particular, in the optical setting, the interaction of discrete solitary waves with structural defects was examined in [21], while "nonstandard" solitary waves (discrete gap solitons) were observed in binary waveguide arrays [22,23]. This activity has been recently reviewed in [24], discussing various aspects of "optics in nonhomogeneous waveguide arrays."

On the BEC side, there are also similar developments involving not only the (attractive or repulsive) localized "defect" action of a laser beam on the condensate [25,26], but also the potential of creating the so-called "superlattice" structures by means of the superposition of optical potentials of different periodicity [27].

In this context of inhomogeneous nonlinear dynamical systems, we propose here a setting, which we illustrate to have drastically different dynamical behavior than that we would expect from its homogeneous counterparts. In particular, we impose a spatial pattern on the nonlinearity, having the form of an "interface" between a set of defocusing Kerr waveguides on the one end and a set of focusing Kerr waveguides on the other, separated by a "transient" layer (interface) of a waveguide bearing intermediate properties between the two segments above. This is, in some aspects, reminiscent of the recent proposition in the context of BEC's of spatially dependent nonlinearities (see, e.g., [28–30] and references therein). We show that this setting already presents a wealth of static and dynamical behavior which is very different than its homogeneous analog. Notice that the present setup bears also some resemblances to the recently proposed fiber guide array resonator of [31] (where two focusing patches of waveguides straddle a defocusing patch thereof). Another recently explored setting (experimentally as well as numerically) with some similarities to the present one is that of the so-called surface solitons [32], where a waveguide lattice interfaces with a continuous medium.

We focus on the localized, solitary-wave excitations in the vicinity of the interface. Starting from the so-called anticontinuum limit of zero coupling [33], we show that the existence and stability of the localized solutions in the vicinity of the interface can be quantified for low couplings by means of perturbation theory using the coupling constant as a small parameter. As the coupling between the sites near the interface increases, the phenomenology becomes drastically different, leading the relevant solution branches to a termination through saddle-node bifurcations that would be absent in the corresponding homogeneous limit. Perhaps equally surprisingly, the more extended multipulse solutions appear to survive for larger values of the coupling than the single (or

smaller size) pulse waves, which is again contrary to what is expected from the homogeneous limit. In this stronger-coupling regime, we investigate the properties of the relevant solutions through numerical bifurcation theory and linear stability analysis. We use direct numerical simulations to illustrate the manifestations of the dynamical instabilities of those among the solutions which are found to be dynamically unstable. We believe that this example illustrates the rich diversity of behavior that can be manifested in such inhomogeneous settings.

Our presentation is structured as follows: In Sec. II, we present the setup and analytical results, while in Sec. III, we study the model numerically and compare with the analytical results. Finally, in Sec. IV, we summarize our findings and present our conclusions.

II. SETUP AND ANALYTICAL RESULTS

We consider an inhomogeneous lattice model described by a discrete nonlinear Schrödinger equation of the following form:

$$i\frac{du_n}{dt} = -C\Delta_2 u_n - d_n|u_n|^2 u_n, \tag{2.1}$$

where C is the coupling between the adjacent sites of the lattice and $\Delta_2 u_n=(u_{n+1}+u_{n-1}-2u_n)$ is the discrete Laplacian. The evolution variable is the propagation distance z in the optical case and the time t in the BEC case; for notational simplicity, we use t in what follows. The nonlinearity coefficient d_n (where n is the spatial index) is determined by the intensity-dependent refractive index (in the context of optics) or the s-wave scattering length (in the context of BEC's) of each waveguide (or optical lattice well for BEC's). The center site d_0 is assumed to have an intermediate value slightly greater than zero. For all $n<0$, the refractive index is set to the defocusing value $d_n=-0.9$. For all $n>0$, the refractive index is set to the focusing value $d_n=1.1$. Note that d_0 is set to the average of these two values—i.e., to 0.1; it should also be mentioned that the results reported below were found to be typical of similar choices of the d_n profile.

We focus our attention on standing wave solutions of the form of $u_n=e^{i\Lambda t}v_n$, where Λ is the propagation constant in optics or the chemical potential in BEC's and v_n is the spatial (time-independent) profile, satisfying the steady-state equation

$$G(v_n,C) \equiv \Lambda v_n - C\Delta_2 v_n - d_n|v_n|^2 v_n = 0. \tag{2.2}$$

It can be easily seen (see, e.g., Refs. [34,35]) that, without loss of generality, we can restrict ourselves to the class of real solutions of Eq. (2.2). In the anticontinuum (AC) limit—i.e., for $C=0$—the solutions are immediately obtainable in the form $v_n^2=\{0,\frac{\Lambda}{d_n}\}$, provided that $\Lambda d_n>0$ for all n. Using this solution and setting to nonzero values only specific individual sites for $n\geqslant 0$, we prescribe the configurations (in the AC limit) for the various branches that will be subsequently examined analytically as well as numerically. The selected configurations are as follows: lower first branch $|1\rangle$, single excited site at $n=0$; upper first branch $|1,e\rangle$, excited sites at $n=0$ and $n=1$ in phase; lower second branch $|1,-e\rangle$, excited sites $n=0$ and $n=1$ but out of phase; and upper second branch $|1,-e,-e\rangle$, excited sites $n=0$ with positive sign and $n=1,2$ with negative signs. Following the same pattern, the remaining branches are lower third branch $|1,-e,e\rangle$, upper third branch $|1,-e,e,e\rangle$, lower fourth branch $|1,-e,e,-e\rangle$, upper fourth branch $|1,-e,e,-e,-e\rangle$, lower fifth branch $|1,-e,e,-e,e\rangle$, and upper fifth branch $|1,-e,e,-e,e,e\rangle$.

On the numerical side, we analyze these branches using the pseudoarclength continuation method [36]. This allows us to trace the branches past fold points and has the significant advantage that it automatically traces the unstable branch corresponding to a certain stable branch. Furthermore, it gives a systematic and accurate way of computing the turning point of the relevant saddle-node bifurcation associated with such folds. In particular, given a solution $(\vec{v}_0,C_0)$ of Eq. (2.2), $G(\vec{v},C)=0$, and a direction vector $(\dot{\vec{v}}_0,\dot{C}_0)$, one can determine $(\vec{v}_1,C_1)$ by solving the following system of equations:

$$G(\vec{v}_1,C_1)=0,$$

$$(\vec{v}_1-\vec{v}_0)\dot{\vec{v}}_0+(C_1-C_0)\dot{C}_0-\Delta s=0, \tag{2.3}$$

where Δs is a (small) arclength parameter. We use Newton's method to solve the system in Eq. (2.3) for $(\vec{v}_1,C_1)$:

$$\begin{pmatrix} \frac{\partial}{\partial\vec{v}}G & \frac{\partial}{\partial C}G \\ \dot{\vec{v}}_0 & \dot{C}_0 \end{pmatrix}\begin{pmatrix} \vec{v}_1^{(new)}-\vec{v}_0 \\ C_1^{(new)}-C_0 \end{pmatrix} = -\begin{pmatrix} G(\vec{v}_1,C_1) \\ (\vec{v}_1-\vec{v}_0)\dot{\vec{v}}_0+(C_1-C_0)\dot{C}_0-\Delta s \end{pmatrix}. \tag{2.4}$$

The next (normalized) direction vector $(\dot{\vec{v}}_1,\dot{C}_1)$ can be computed by solving

$$\begin{pmatrix} \frac{\partial}{\partial\vec{v}}G & \frac{\partial}{\partial C}G \\ \dot{\vec{v}}_0 & \dot{C}_0 \end{pmatrix}\begin{pmatrix} \dot{\vec{v}}_1 \\ \dot{C}_1 \end{pmatrix} = \begin{pmatrix} 0 \\ 1 \end{pmatrix}. \tag{2.5}$$

To examine the linear stability of the stationary solutions obtained as described above, we use the perturbation ansatz

$$u_n = e^{i\Lambda t}(v_n + \epsilon a_n e^{-i\omega t} + \epsilon b_n e^{i\omega^* t}), \tag{2.6}$$

where ϵ is a formal small parameter. By substituting Eq. (2.6) into Eq. (2.1) and dropping higher-order terms, the following system of linear stability equations is obtained:

$$\omega a_n = -C\Delta_2 a_n + \Lambda a_n - 2d_n|v_n|^2 a_n - d_n v_n^2 b_n^*,$$

$$\omega^* b_n = C\Delta_2 b_n - \Lambda b_n + 2d_n|v_n|^2 b_n + d_n v_n^2 a_n^*. \tag{2.7}$$

The numerical solution of the ensuing matrix eigenvalue problem for the eigenfrequencies ω and eigenvectors $\{a_n,b_n^*\}$ can be then used to characterize the linear stability (more precisely the spectral stability) of the solutions. Since the eigenvalues (eigenfrequencies) of the underlying Hamil-

tonian system appear in quartets, to ensure a spectral instability it suffices for the above linear system to possess an eigenfrequency with a nonzero imaginary part. When the solutions are found to be unstable, we use a fourth-order, direct integration scheme to examine the dynamical evolution of the instability.

Having presented the main framework and numerical methods, we now turn to some analytical results. Our analysis will be based on perturbation theory from the anticontinuum limit, using the coupling strength C as the small parameter. In particular, we expand the solution as

$$v_n = v_n^{(0)} + Cv_n^{(1)} + O(C^2). \tag{2.8}$$

It is easy to check that the stability problem of Eq. (2.7) can be rewritten for the eigenvalues $\lambda = i\omega$ in the Hamiltonian form

$$\mathcal{J}\mathcal{H}\psi = \lambda\psi, \tag{2.9}$$

where ψ is the infinite-dimensional eigenvector, consisting of 2-blocks of $(u_n, w_n)^T$ (the superscript T denotes transpose), where $a_n = u_n + iw_n$, $b_n = u_n - iw_n$ for the eigenvector equations (2.7), $\mathcal{J}$ is the infinite-dimensional skew-symmetric matrix, which consists of 2×2 blocks of

$$\mathcal{J}_{n,m} = \begin{pmatrix} 0 & 1 \\ -1 & 0 \end{pmatrix} \delta_{n,m},$$

and $\mathcal{H}$ is the infinite-dimensional symmetric matrix, which consists of 2×2 blocks of

$$\mathcal{H}_{n,m} = \begin{pmatrix} (\mathcal{L}_+)_{n,m} & 0 \\ 0 & (\mathcal{L}_-)_{n,m} \end{pmatrix}.$$

The matrices $(\mathcal{L}_+)_{n,m}$ and $(\mathcal{L}_-)_{n,m}$ are, in turn, defined as

$$(\mathcal{L}_+)_{n,n} = 1 - 3d_n v_n^2, \quad (\mathcal{L}_-)_{n,n} = 1 - d_n v_n^2,$$

$$(\mathcal{L}_\pm)_{n,n+1} = (\mathcal{L}_\pm)_{n+1,n} = -C.$$

Similarly to the solution itself, the matrix $\mathcal{H}$ in the neighborhood of the AC limit can be expanded as

$$\mathcal{H} = \mathcal{H}^{(0)} + \sum_{k=1}^{\infty} C^k \mathcal{H}^{(k)}, \tag{2.10}$$

where $\mathcal{H}^{(0)}$ is diagonal with two blocks:

$$\mathcal{H}_{n,n}^{(0)} = \begin{pmatrix} -2 & 0 \\ 0 & 0 \end{pmatrix}, \quad n \in S, \quad \mathcal{H}_{n,n}^{(0)} = \begin{pmatrix} 1 & 0 \\ 0 & 1 \end{pmatrix} \quad , n \in \mathbb{Z} \setminus S, \tag{2.11}$$

where S denotes the set of excited sites. Notice that in the $C=0$ limit, each excited site corresponds to a pair of zero eigenvalues in Eq. (2.9), while each zero site corresponds to a pair of eigenvalues at ± 1.

Choosing for simplicity of exposition (and without loss of generality) $\Lambda + 2C = 1$ in Eq. (2.2), the solution of the leading order perturbation problem in Eq. (2.8) is governed by the following equation:

$$[1 - 3d_n (v_n^{(0)})^2] v_n^{(1)} = v_{n+1}^{(0)} + v_{n-1}^{(0)}. \tag{2.12}$$

One can apply this, e.g., for the two-site solutions such as $|1, e\rangle$ and $|1, -e\rangle$, to obtain the leading-order corrections

$$v_0^{(1)} = -\frac{1}{2}\left(\pm\sqrt{\frac{1}{d_1}}\right), \tag{2.13}$$

$$v_1^{(1)} = -\frac{1}{2}\left(\pm\sqrt{\frac{1}{d_0}}\right), \tag{2.14}$$

where the sign inside the parentheses corresponds to the sign of excitation of the site indexed inside the square root. Similarly, for three excited sites the expressions become

$$v_0^{(1)} = -\frac{1}{2}\left(\pm\sqrt{\frac{1}{d_1}}\right), \tag{2.15}$$

$$v_1^{(1)} = -\frac{1}{2}\left(\pm\sqrt{\frac{1}{d_0}} \pm \sqrt{\frac{1}{d_2}}\right), \tag{2.16}$$

$$v_2^{(1)} = -\frac{1}{2}\left(\pm\sqrt{\frac{1}{d_1}}\right). \tag{2.17}$$

One can correspondingly generalize these expressions for an arbitrary number of excited sites.

We now turn to the perturbed stability problem. The small perturbation of size C cannot render the eigenvalues of order $O(1)$ unstable. Instead, the potentially "dangerous" eigenvalues for instability purposes are those which are located at the origin of the spectral plane in the AC limit (corresponding to the excited sites, as discussed above). The perturbed form $\mathcal{H}_1$ of the matrix relevant to the stability problem can be easily seen (from the perturbative expansion) to assume the form

$$\mathcal{H}_{n,n}^{(1)} = -2d_n \phi_n^{(0)} \phi_n^{(1)} \begin{pmatrix} 3 & 0 \\ 0 & 1 \end{pmatrix}, \quad \mathcal{H}_{n,n+1}^{(1)} = \mathcal{H}_{n+1,n}^{(1)} = -\begin{pmatrix} 1 & 0 \\ 0 & 1 \end{pmatrix}, \tag{2.18}$$

while all other blocks of $\mathcal{H}_{n,m}^{(1)}$ are zero. If we consider the (linearly independent) eigenvectors corresponding to zero eigenvalues of $\mathcal{H}_0$, $\mathbf{f}_n$, then it was proved in [35] that in order to obtain the leading correction to the (zero) eigenvalues of the original problem, it is sufficient to consider the reduced problem

$$\mathcal{M}_1 \mathbf{c} = \gamma_1 \mathbf{c}, \tag{2.19}$$

where

$$(\mathcal{M}_1)_{m,n} = (\mathbf{f}_m, \mathcal{H}^{(1)} \mathbf{f}_n) \tag{2.20}$$

is an $N\times N$ matrix, with N being the number of excited sites. Once the eigenvalues γ_1 of this reduced problem are obtained, then the perturbed eigenvalues of the original problem are given by $\lambda = \sqrt{C}\lambda_1 + O(C)$, where $\lambda_1 = \sqrt{2\gamma_1}$. It is worthwhile to note here that the above-described analysis of the stability problem also bears deep resemblances to a similar (finite-dimensional matrix) reduction for the breather stability problem performed for Klein-Gordon lattices in [37] (see also [38]).

One can then directly compute the matrix $\mathcal{M}$, e.g. in the two-site and three-site cases, as well as more generally, to have the forms

$$(\mathcal{M})_{n,n} = -2d_n v_n^{(0)} v_n^{(1)}, \quad (\mathcal{M})_{n,n-1} = -\cos(\theta_{n-1} - \theta_n),$$

$$(\mathcal{M})_{n,n+1} = -\cos(\theta_{n+1} - \theta_n).$$

One can then obtain the following predictions for the leading-order eigenvalues of some of the branches discussed above (we only explicitly present these predictions in the two- and three-site cases),

$$\lambda = \pm 2.69003\sqrt{C}, \tag{2.21}$$

$$\lambda = \pm 2.69003i\sqrt{C}, \tag{2.22}$$

for the (unstable) $|1,e\rangle$ and (stable, at least for small C) $|1,-e\rangle$ modes, respectively. In the three-site case, we have the following.

(i) For the branch $|1,e,e\rangle$, two real eigenvalue pairs

$$\lambda_1 = \pm 1.277714\sqrt{C}, \quad \lambda_2 = \pm 3.098986\sqrt{C}. \tag{2.23}$$

(ii) For the branch $|1,-e,e\rangle$, the same eigenvalue pairs as above but multiplied by i (hence the branch is marginally stable for small C).

(iii) For the branch $|1,e,-e\rangle$, one real and one imaginary pair in the form

$$\lambda_1 = \pm 1.63075i\sqrt{C}, \quad \lambda_2 = \pm 2.428092\sqrt{C}. \tag{2.24}$$

(iv) Similarly, the branch $|1,-e,-e\rangle$ has the same eigenvalues as $|1,e,-e\rangle$ but multiplied by i (so it is also always linearly unstable).

Notice that one can, in principle, expand this type of analysis to any other configuration of interest.

We now turn to numerical results in order to examine the validity of these theoretical predictions.

III. NUMERICAL RESULTS

Figure 1 summarizes our essential numerical results, presenting the squared l^2 norm of the solution (physically, the power in optics or the rescaled number of atoms in BEC) $P=\Sigma_n|u_n|^2$ for the various branches that we examined in our computations. (For the explanation of the branches that are shown, the reader is referred to Sec. II.) For convenience herein P is scaled by a factor of 0.15. There are a number of features in this bifurcation diagram which are in extreme contrast with the corresponding homogeneous limit of this system. First, the single-pulse branch in the vicinity of the interface already terminates for quite small values of C; in fact, it is the first branch to terminate in a saddle-node bifurcation with the two-site mode $|1,e\rangle$. This is the analog of what would be termed the "Page mode" in the setting of intrinsic localized modes (ILM's). As the coupling increases, the site with index $n=1$ starts becoming excited for the single-pulse branch, eventually colliding (in configuration space) with the two-site mode and annihilating each other. In the homogeneous limit of a focusing medium both of these

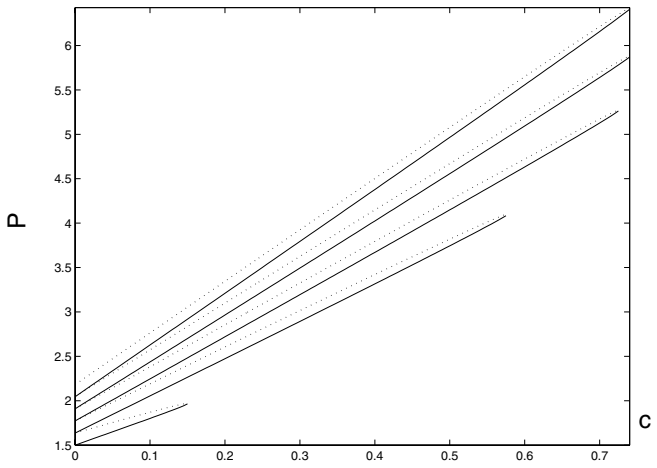

FIG. 1. Bifurcation diagram of the first five branches. Plot of the solution's scaled power P as a function of the continuation parameter C. Dotted lines represent unstable regions. Solid lines represent initially stable regions.

branches would survive for *any* C, up to the continuum limit of $C\to\infty$. A similar phenomenology emerges for the so-called twisted mode branch of $|1,-e\rangle$, which, in turn, is also linearly stable for small C; for larger C, it eventually collides with the branch $|1,-e,-e\rangle$ and disappears in a saddle-node bifurcation. The same is also true for the pair of $|1,-e,e\rangle$ and $|1,-e,e,e\rangle$ and for that of $|1,-e,e,-e\rangle$ and $|1,-e,e,-e,-e\rangle$ also shown in the figure. Another interesting general trend illustrated in this diagram is that the more extended the branch (i.e., the more sites participating in the nonlinear wave), the larger the coupling strength for which it persists. This is also contrary to what one would expect from the homogeneous limit, where multisite solutions can only be continued to a finite coupling which is typically larger for more localized structures.

Figure 2 illustrates the details of the lower pair of branches in Fig. 1. In particular, panel (a) shows the profile of the modes and their corresponding stability for the stable $|1\rangle$ and unstable $|1,e\rangle$ solutions. The continuation of the branches (up to $C=0.15$ where they collide and disappear) is shown in detail. The instability of the unstable two-site solution is investigated in panel (b) through a direct simulation showing its breathing evolution. In these types of numerical experiments, throughout the text, the lattice is initialized with the unstable configuration (without any additional perturbation). The truncation error due to the finite accuracy of the solution is eventually amplified to O(1), manifesting the instability of the configuration. Panel (c) reports the result of the full numerical simulation (solid line) versus the theoretical prediction (dashed line), for both the instability eigenvalue of $|1,e\rangle$ and the profile correction imposed by Eqs. (2.13) and (2.14). It is readily observed that, for small values of C, the agreement between the analytical predictions and the numerical results is very good. Of course, for larger C, the analytical results are expected to be less successful due to the significance of higher-order corrections neglected in our analysis.

Figure 3 is similar to Fig. 2, but for the second pair of solutions in Fig. 1: namely, for $|1,-e\rangle$ and its corresponding

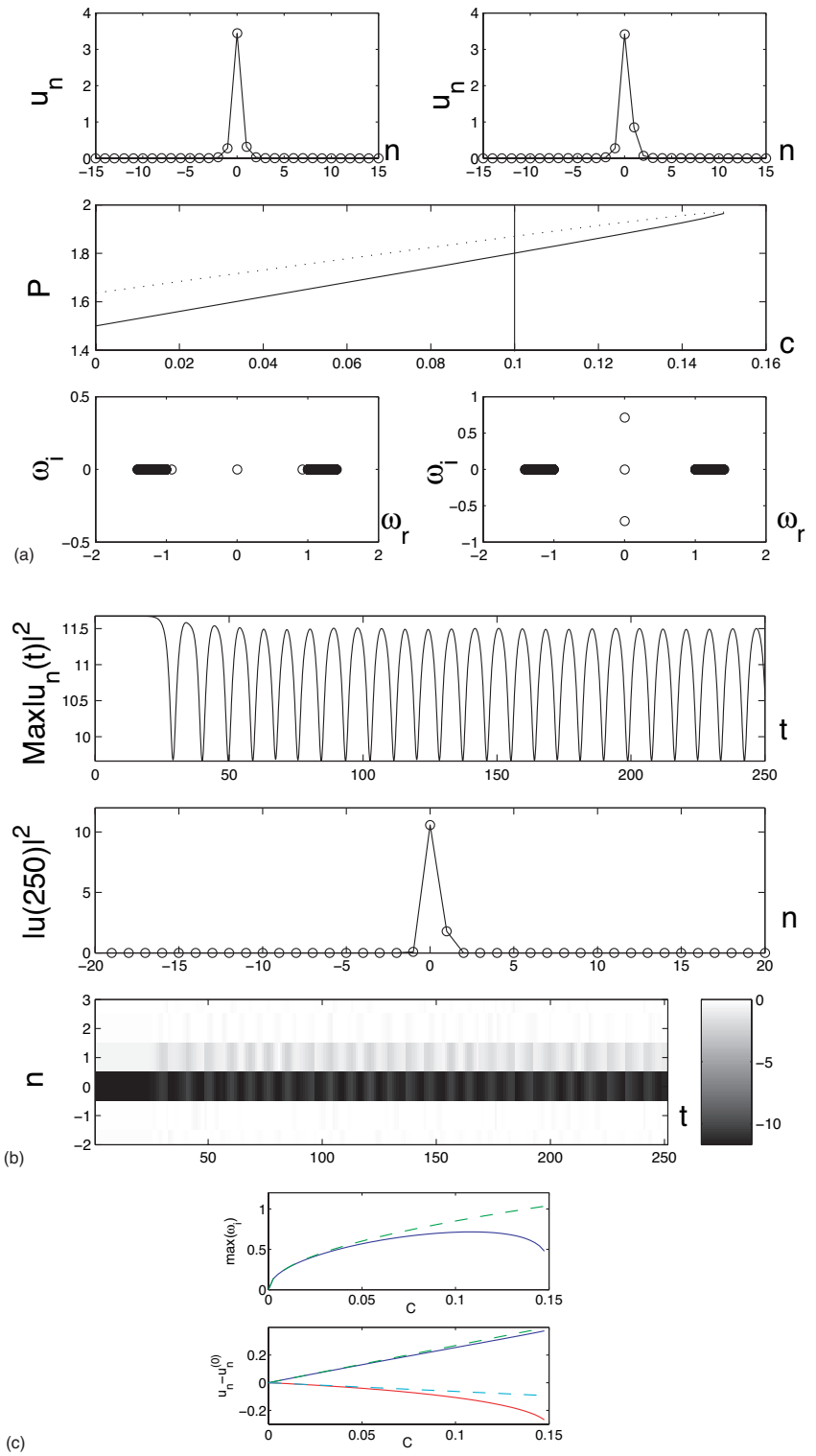

FIG. 2. (Color online) (a) Profiles of wave configurations and eigenfrequencies at the value of $C=0.1$ where the solid vertical line crosses branch one in the center diagram. Upper left: wave configuration from lower half of branch one, segment $|1\rangle$. Lower left: eigenfrequencies of the linearization around this solution. Upper right: wave configuration from upper half of branch one, segment $|1,e\rangle$. Lower right: eigenfrequencies from the corresponding linearization. (b) Top: evolution of the maximum of the square modulus of the solution taken from the upper branch at $C=0.1$. Middle: spatial profile of the square modulus of u taken for $C=0.1$, after propagation of 250 time units. Bottom: space-time contour plot of the square modulus of the solution. (c) The top panel shows the most unstable eigenvalue of the two-site solution of $|1,e\rangle$ as a function of the coupling strength C. The solid line is the full numerical result, while the dashed line denotes the analytical prediction. The bottom panel shows the correction for the central site $n=0$ and its neighboring site $n=1$ given by the first-order theory (dashed line) versus the corresponding numerical result (solid line).

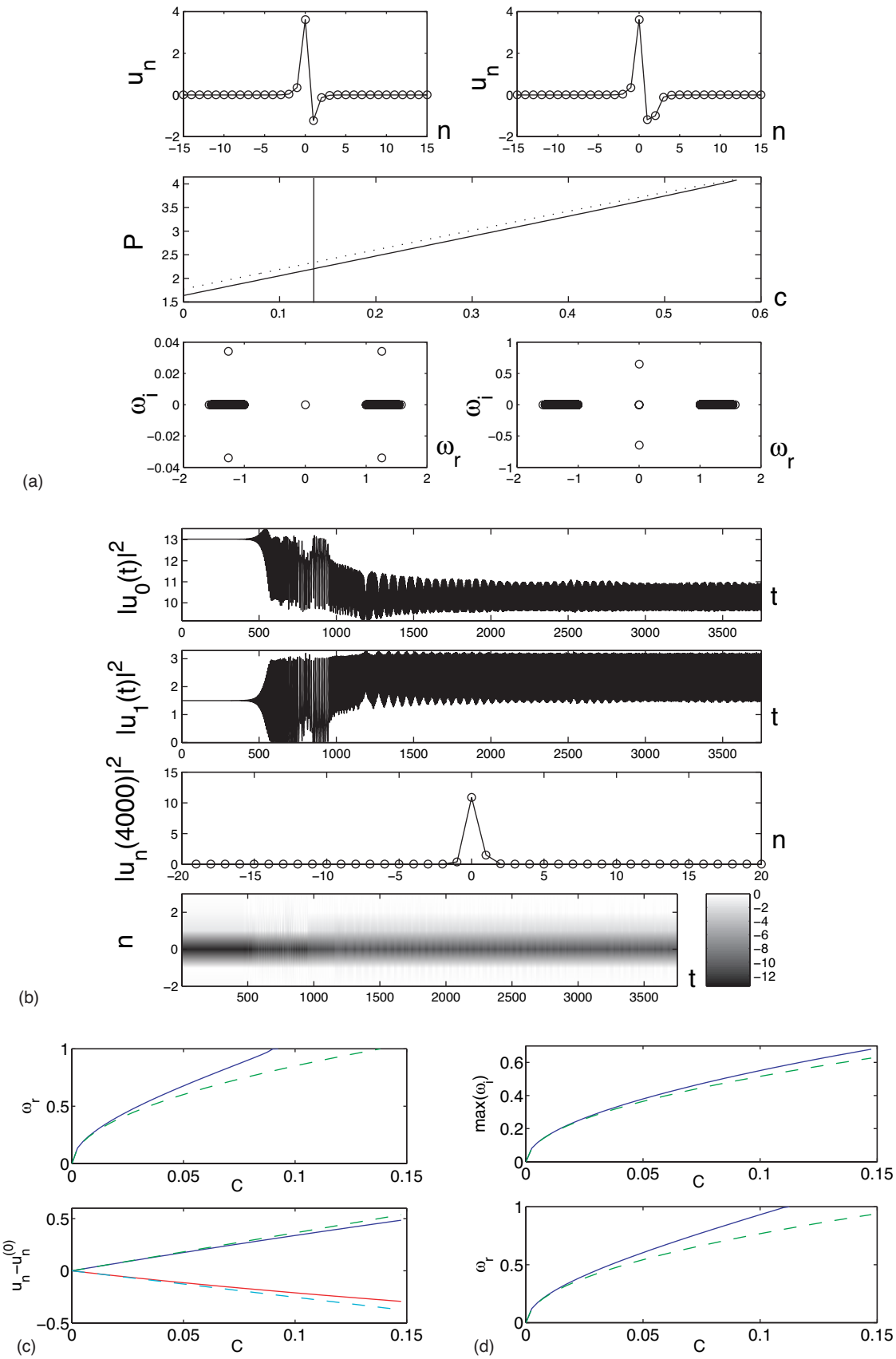

FIG. 3. (Color online) (a) Similar to Fig. 2 for the second branch, with profiles at $C=0.135$, for the segments $|1,-e\rangle$ and $|1,-e,-e\rangle$. (a)–(c) are similar as above, while panel (d) shows the eigenfrequencies (one real and one imaginary, as predicted by theory) of the mode $|1,-e,-e\rangle$ from the numerical results (solid) against the analytical predictions of Sec. II (dashed lines).

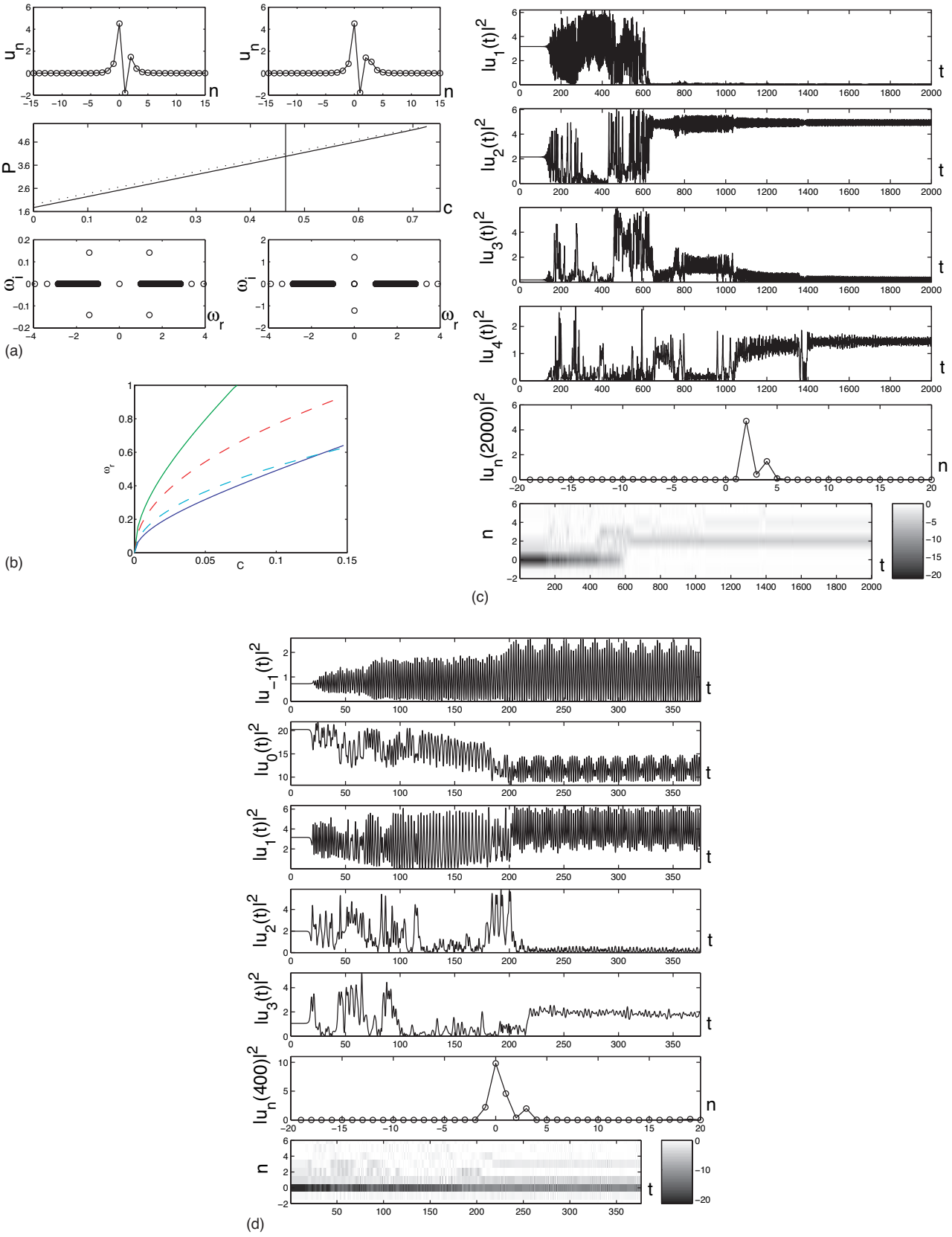

FIG. 4. (Color online) Panel (a) shows the profiles and eigenfrequencies of the third branch ($|1,-e,e\rangle$ on the left and $|1,-e,e,e\rangle$ on the right) for $C=0.465$. Panel (b) shows, for the three-site mode $|1,-e,e\rangle$, the dependence of its two eigenfrequencies against the analytical predictions (dashed lines). Panels (c) and (d) show, for each of the branches and for $C=0.465$, the dynamical evolution of the principal sites, as well as the space-time contour plot of the square modulus.

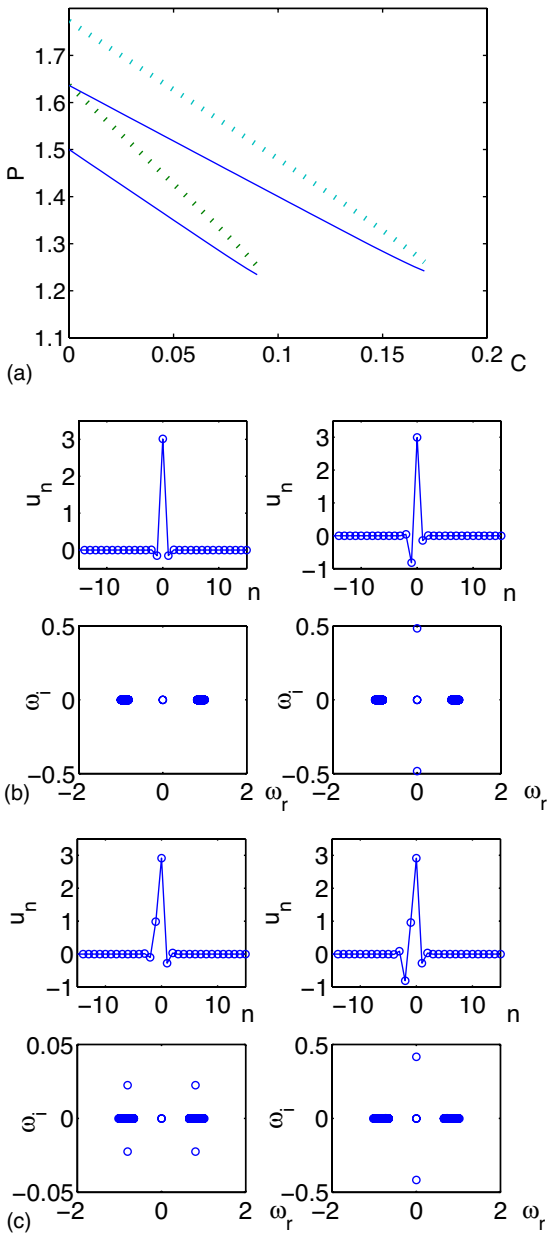

FIG. 5. (Color online) (a) The top panel shows the bifurcation diagram of the scaled power P versus C for the first pair of branches in the defocusing case with $\Lambda=-1$. Similarly to Fig. 1, the solid lines denote the stable branches and the dotted lines the unstable ones. (b) The single site (left panels) and two-site, out of phase (right panels) branches that eventually collide with each other in the defocusing case are shown for $C=0.045$. The top panels show the branches' profile and bottom ones their respective stability. (c) Similarly for the second pair of colliding branches: namely, the two-site in phase and the corresponding three-site branch, both of which are shown for $C=0.085$.

unstable companion $|1,-e,-e\rangle$. These branches disappear together in a saddle-node bifurcation for $C=0.575$. While $|1,-e,-e\rangle$ is always unstable due to a real eigenvalue for any C, the twisted mode is stable for small C, but becomes unstable for $C>0.095$ due to the collision of two imaginary eigenvalue pairs with opposite Krein signature, leading to a quartet of eigenvalues through a Hamiltonian Hopf bifurcation [39]. Panel (a) of the figure illustrates the solution profiles, the bifurcation diagram, and the results of the stability analysis. Panel (b) highlights the breathing evolution of the twisted-mode state. Panels (c) and (d) compare the eigenvalue prediction of Eq. (2.22) with the full numerical result (dashed versus solid lines) and the leading-order correction for the two side modes, in the case of the left panel. In the right panel, the eigenvalue predictions (one real and one imaginary) for the $|1,-e,-e\rangle$ branch (dashed line) are also compared to the corresponding numerical results (solid line), obtaining once again good agreement.

In Fig. 4, we examine the third pair of branches of Fig. 1: namely (stable for small C), $|1,-e,e\rangle$ and (always unstable) $|1,-e,e,e\rangle$. These branches, in turn, collide and disappear through a saddle node for $C=0.725$. Panel (b) shows the prediction (dashed line) versus the numerical results (solid line) for the leading-order eigenvalues of the $|1,-e,e\rangle$ solution (discussed in the previous section). The theory correctly captures, at small C, the existence of two imaginary eigenvalues and their $C^{1/2}$ bifurcation from 0, but is somewhat less satisfactory quantitatively in this case. This branch becomes unstable around $C=0.08$ due to the collision of one of these eigenvalue pairs with one of opposite Krein signature, leading once again to a quartet of eigenvalues. The details of the subsequent dependence of this unstable eigenvalue on C, for both this branch and $|1,-e\rangle$, depend also on the size of the domain for reasons similar to those discussed in [40]. The two bottom panels show the unstable evolution of the corresponding solutions, illustrating an interesting phenomenon particularly in the case of the $|1,-e,e\rangle$ branch. The dynamical evolution favors the tunneling of the excitation from the position of the interface to a nearby site (in this case, mainly to $n=2$). That is, the interface displaces the solution towards a position where the environment is more conducive (being surrounded by focusing sites) to the existence of a localized pulse solution.

Defocusing excitations

So far, our discussion has been limited to the excitations occurring on the focusing side of the interface. However, it is, of course, possible to have similar excitations on the defocusing side of the interface. We now briefly discuss the latter setting.

First, we note that in discrete nonlinear Schrödinger systems, there exists the so-called staggering transformation $v_n=(-1)^n u_n$, which converts a focusing problem to a defocusing one (and vice versa), up to a shift in the excitation frequency which can always be absorbed through a phase transformation. Hence, upon using such a staggering transformation, one realizes immediately that the phenomenology of the interface problem should remain essentially similar if the excitations emerge on the defocusing side of the interface. The main difference emerging from the above transformation is that the on-site branch will collide with the $|1,-e\rangle$ branch (rather than with the $|1,e\rangle$ one), the $|1,e\rangle$ branch colliding with the $|1,e,-e\rangle$ branch (rather than the $|1,-e\rangle$ colliding with the $|1,-e,-e\rangle$ one). Thus, the modified bifurcations and stability properties can be qualitatively identified by means of this transformation.

However, for reasons of completeness we have also corroborated the above statements with typical numerical computations in the latter regime. We start by noting that for excitations on the defocusing side of the domain, it is evident from the anticontinuum limit that the excitation's propagation constant Λ would have to be negative. Furthermore, for the localized multisite excitations near the interface considered herein, we have used an appropriately modified form of the inhomogeneous nonlinear coefficients d_n, with $d_n=-1.1$ and $n<0$, $d_0=-0.1$ and $d_n=0.9$ for $n>0$. The first two relevant saddle-node bifurcations and the branches corresponding to these are then shown in Fig. 5, confirming the above predictions concerning the participating branches. We note in passing the fact that the turning points ($C\approx 0.093$ and $C\approx 0.174$, respectively, for the bifurcations shown in Fig. 5) occur for different values of C than in the focusing case which is due to the "renormalization" of the propagation constant imposed by the staggering transformation.

IV. CONCLUSIONS

In the present paper, we have introduced a setting for the study of the recent theme of inhomogeneous nonlinear lattices in nonlinear optics (waveguide arrays) and Bose-Einstein condensates (optical lattices and superlattices). The setting consists of an interface between defocusing and focusing (repulsive interaction and attractive interaction, respectively) regions and a transient layer between the two.

We have focused specifically on the statics and dynamics of coherent wave forms in the vicinity of this interface, and we have found that their properties are dramatically modified in comparison with those expected from the homogeneous case. Some manifestations of these differences can be quantified in the termination of the principal pulse branch (for small couplings) or the more prolonged (in parameter space) persistence of more extended structures in comparison with more localized ones. Furthermore, we have shown that the interface may induce a dynamical tunneling of the structures towards locations more favorable for their existence. We have also developed a systematic methodology based on the adaptation of the considerations of [35] to inhomogeneous settings and illustrated how to use these to develop a perturbative treatment of the problem with excellent qualitative and good quantitative agreement with the full numerical results.

There are many interesting questions that are suggested for the interface problem we have introduced. A prominent one concerns the dynamical evolution of coherent structures moving towards the interface and their interaction with (transmission through, reflection from or trapping at) that region.

ACKNOWLEDGMENTS

Research at LANL is conducted under the auspices of the U.S. DOE. One of the authors (P.G.K.) gratefully acknowledges the support of Grants Nos. NSF-DMS-0204585, NSF-DMS-0505663, and NSF-CAREER, as well as informative discussions with J. Leon.

[1] H. S. Eisenberg, R. Morandotti, Y. Silberberg, J. M. Arnold, G. Pennelli, and J. S. Aitchison, J. Opt. Soc. Am. B **19**, 2938 (2002).
[2] U. Peschel, R. Morandotti, J. M. Arnold, J. S. Aitchison, H. S. Eisenberg, Y. Silberberg, T. Pertsch, and F. Lederer, J. Opt. Soc. Am. B **19**, 2637 (2002).
[3] N. K. Efremidis, S. Sears, D. N. Christodoulides, J. W. Fleischer, and M. Segev, Phys. Rev. E **66**, 046602 (2002).
[4] A. A. Sukhorukov, Yu. S. Kivshar, H. S. Eisenberg, and Y. Silberberg, IEEE J. Quantum Electron. **39**, 31 (2003).
[5] F. S. Cataliotti, S. Burger, C. Fort, P. Maddaloni, F. Minardi, A. Trombettoni, A. Smerzi, and M. Inguscio, Science **293**, 843 (2001).
[6] F. S. Cataliotti, L. Fallani, F. Ferlaino, C. Fort, P. Maddaloni, and M. Inguscio, New J. Phys. **5**, 71 (2003).
[7] F. Kh. Abdullaev, B. B. Baizakov, S. A. Darmanyan, V. V. Konotop, and M. Salerno, Phys. Rev. A **64**, 043606 (2001).
[8] G. L. Alfimov, P. G. Kevrekidis, V. V. Konotop, and M. Salerno, Phys. Rev. E **66**, 046608 (2002).
[9] M. V. Fistul, Chaos **13**, 725 (2003).
[10] J. J. Mazo and T. P. Orlando, Chaos **13**, 733 (2003).
[11] T. Dauxois, M. Peyrard, and A. R. Bishop, Phys. Rev. E **47**, R44 (1993).
[12] M. Peyrard, T. Dauxois, H. Hoyet, and C. R. Willis, Physica D **68**, 104 (1993).
[13] S. Aubry, Physica D **103**, 201 (1997).
[14] S. Flach and C. R. Willis, Phys. Rep. **295**, 181 (1998).
[15] D. Hennig and G. Tsironis, Phys. Rep. **307**, 333 (1999).
[16] P. G. Kevrekidis, K. O. Rasmussen, and A. R. Bishop, Int. J. Mod. Phys. B **15**, 2833 (2001).
[17] J. Ch. Eilbeck and M. Johansson, in *Localization and Energy Transfer in Nonlinear Systems*, edited by L. Vazquez, R. S. MacKay, and M. P. Zorzano (World Scientific, Singapore, 2003), p. 44.
[18] D. N. Christodoulides and R. I. Joseph, Opt. Lett. **13**, 794 (1988).
[19] D. N. Christodoulides, F. Lederer, and Y. Silberberg, Nature (London) **424**, 817 (2003).
[20] A. Trombettoni and A. Smerzi, Phys. Rev. Lett. **86**, 2353 (2001).
[21] R. Morandotti, H. S. Eisenberg, D. Mandelik, Y. Silberberg, D. Modotto, M. Sorel, C. R. Stanley, and J. S. Aichison, Opt. Lett. **28**, 834 (2003).
[22] R. Morandotti, D. Mandelik, Y. Silberberg, J. S. Aitchison, M. Sorel, D. N. Christodoulides, A. A. Sukhorukov, and Yu. S. Kivshar, Opt. Lett. **29**, 2890 (2004).
[23] D. Mandelik, R. Morandotti, J. S. Aitchison, and Y. Silberberg, Phys. Rev. Lett. **92**, 093904 (2004).
[24] R. Morandotti, H. S. Eisenberg, D. Mandelik, Y. Silberberg, D. Modotto, M. Sorel, C. R. Stanley, and J. S. Aitchison, Opto-

Electron. Rev. **13**, 103 (2005).
[25] C. Raman, M. Kohl, R. Onofrio, D. S. Durfee, C. E. Kuklewicz, Z. Hadzibabic, and W. Ketterle, Phys. Rev. Lett. **83**, 2502 (1999).
[26] R. Onofrio, C. Raman, J. M. Vogels, J. R. Abo-Shaeer, A. P. Chikkatur, and W. Ketterle, Phys. Rev. Lett. **85**, 2228 (2000).
[27] S. Peil, J. V. Porto, B. L. Tolra, J. M. Obrecht, B. E. King, M. Subbotin, S. L. Rolston, and W. D. Phillips, Phys. Rev. A **67**, 051603(R) (2003).
[28] G. Theocharis, P. Schmelcher, P. G. Kevrekidis, and D. J. Frantzeskakis, Phys. Rev. A **72**, 033614 (2005).
[29] G. Theocharis, P. Schmelcher, P. G. Kevrekidis, and D. J. Frantzeskakis, e-print cond-mat/0509471.
[30] H. Sakaguchi and B. A. Malomed, Phys. Rev. E **72**, 046610 (2005).
[31] J. Leon, Phys. Rev. E **70**, 056604 (2004).
[32] S. Suntsov, K. G. Makris, D. N. Christodoulides, G. I. Stegeman, A. Haché, R. Morandotti, H. Yang, G. Salamo, and M. Sorel, Phys. Rev. Lett. **96**, 063901 (2006).
[33] R. S. MacKay and S. Aubry, Nonlinearity **7**, 1623 (1994).
[34] G. L. Alfimov, V. A. Brazhnyi, and V. V. Konotop, Physica D **194**, 127 (2004).
[35] D. E. Pelinovsky, P. G. Kevrekidis, and D. J. Frantzeskakis, Physica D **212**, 1 (2005).
[36] E. J. Doedel, http://indy.cs.concordia.ca/auto
[37] J. Cuevas, J. F. R. Archilla, and F. R. Romero, Nonlinearity **18**, 769 (2005).
[38] J. F. R. Archilla, J. Cuevas, B. Sánchez-Rey, and A. Álvarez, Physica D **180**, 235 (2003).
[39] J.-C. van der Meer, Nonlinearity **3**, 1041 (1990).
[40] M. Johansson and Yu. S. Kivshar, Phys. Rev. Lett. **82**, 85 (1999).